Adv. Manuf. (2020) 8:440–446
https://doi.org/10.1007/s40436-020-00324-z

Nanometric polishing of lutetium oxide by plasma-assisted etching

Peng Lyu[1] · Min Lai[1] · Feng-Zhou Fang[1,2]

Received: 30 January 2020 / Revised: 10 July 2020 / Accepted: 15 September 2020 / Published online: 3 November 2020
© The Author(s) 2020

Abstract Plasma-assisted etching, in which the irradiation of hydrogen plasma and inorganic acid etching are integrated, is proposed as a novel polishing method for sesquioxide crystals. By means of this approach, low damage and even damage-free surfaces with a high material removal rate can be achieved in lutetium oxide surface finishing. Analysis of transmission electron microscopy and X-ray photoelectron spectroscopy reveal that plasma hydrogenation converts the sesquioxide into hydroxide, which leads a high efficient way to polish the surfaces. The influences of process conditions on the etching boundary and surface roughness are also qualitatively investigated using scanning electron microscope and white light interferometry. The newly developed process is verified by a systematic experiment.

Keywords Plasma-assisted etching · Lutetium oxide · Surface roughness · Subsurface damage

✉ Min Lai
laimin@tju.edu.cn

✉ Feng-Zhou Fang
fzfang@tju.edu.cn

[1] State Key Laboratory of Precision Measuring Technology and Instruments, Centre of Micro/Nano Manufacturing Technology (MNMT), Tianjin University, Tianjin 300072, People's Republic of China

[2] Centre of Micro/Nano Manufacturing Technology (MNMT-Dublin), School of Mechanical and Materials Engineering, University College Dublin, Dublin 4, Ireland

1 Introduction

Mid-infrared (mid-IR) laser sources with emission wavelengths from 3 μm to 5 μm, and within the atmospheric window, are promising light sources in the fields of optical communication, remote sensing technology, and semiconductors [1–3]. As this band is in the strong absorption zone of water ($\sim 10^4$ cm^{-1}), the penetration depth when mid-IR light is used to cut through skin or biological tissue is only a few micrometers [4, 5]. The cubic rare-earth sesquioxide crystal, lutetium oxide (Lu_2O_3), is a promising mid-IR laser matrix owing to its excellent properties. The effective phonon energy of Lu_2O_3 is 430 cm^{-1}, which is quite low compared to the host material yttrium aluminum garnet (YAG) at 700 cm^{-1}, implying low nonradiative transition rates and, therefore, higher quantum efficiency [6]. The thermal conductivity of undoped Lu_2O_3 (12.5 W/(m·K)) is higher than that of undoped YAG (11 W/(m·K)). If the crystals are doped with 3% ytterbium ions, the thermal conductivity drops considerably to 6.6 W/(m·K) and 6.8 W·(m·K)$^{-1}$, for Sc_2O_3 and YAG respectively. However, in Lu_2O_3, the thermal conductivity changes only slightly to 11.0 W/(m·K). These properties make Lu_2O_3 attractive for high-power solid-state lasers [7, 8].

To use Lu_2O_3 for high-power laser devices, an atomically smooth and damage-free surface is required. However, Lu_2O_3 is difficult to machine because of its physical properties and chemical inertness. Lu_2O_3 is a hard and brittle material, with a hardness of approximately 10.8 GPa and a melting point up to 2 400 °C [9–11]. It has a strong stability in acid solution. For example, it remains almost unchanged when placed in aqua regia for 24 h. The study of sesquioxide crystal materials mainly focuses on crystal growth, spectral characteristics, and laser properties [12].

At present, no studies on ultrasmooth finishing of Lu_2O_3 have been reported.

Traditional cutting [13, 14], grinding [15], and polishing processes [16] are the main methods of processing laser crystals. These processing methods mainly employ mechanical contact to remove workpiece materials. However, the stability of the machining equipment is an important factor in determining the accuracy of the crystals. It is also affected by external disturbances in the relative displacement between the workpiece and tool owing to vibration and thermal deformation because the surfaces of these crystals are created by a contact removal mechanism [17]. Inevitably, the surface quality and lattice integrity of crystals are damaged because of mechanical machining, resulting in surface/subsurface damage and residual stress, which directly reduces the damage threshold. Therefore, several unconventional noncontact techniques for hard and brittle material with nanometer-level form accuracy have been reported. Namba and Tsuwa [18] proposed float polishing in which a surface roughness 1 nm R_a could be obtained for sapphire single crystals. Mori et al. [19] demonstrated that minute atomic-size removal was achieved with no damage by elastic emission machining. Gormley et al. [20] suggested hydroplane polishing, which produces damage-free surfaces of gallium arsenide and Indium phosphide. Li et al. [21] proposed chemical-mechanical polishing, which is now widely used as the finishing process of 4H-SiC substrates. Kordonski et al. [22] used magnetorheological finishing to reduce the surface roughness of optical glasses to less than 1 nm R_a. Yang et al. [23] used slurryless electrochemical-mechanical polishing to obtain an atomically smooth SiC surface. However, the removal rates of these finishing processes are extremely low. Plasma surface treatment technology can create surfaces that are difficult to achieve with traditional processing methods. Arnold et al. [24] presented plasma jet machining (PJM), a method suitable for optical surfaces of ultralow expansion glass; the volume removal rate was up to 50 mm^3/min and the surface roughness was less than 3 nm R_a. On the other hand, Sun et al. [25] and Yamamura et al. [26] proposed plasma chemical-vaporization machining (PCVM) and plasma-assisted polishing. These plasma technologies remove material by chemical reactions, forming volatile species, or reducing the hardness of modified surfaces, and are mainly used in silicon-based materials. Therefore, it is necessary to develop an efficient finishing process for the ultrasmooth surfaces of sesquioxide crystals.

In this study, a novel finishing approach, i.e., plasma-assisted etching (PaE), combining the irradiation of hydrogen plasma for surface modification and inorganic acid etching for surface removal was used to realize ultrasmooth surfaces of crystal samples. The surface chemical structure of Lu_2O_3 modified by irradiation of hydrogen plasma was investigated by X-ray photoelectron spectroscopy (XPS) and transmission electron microscopy (TEM), and the etching results of Lu_2O_3 using inorganic acid were analyzed.

2 Plasma-assisted etching

In plasma etching processes, such as PJM and PCVM, a damage-free surface can be obtained because of the chemical removal characteristics of this processes [24, 25]. However, these processing methods require the plasma to act on the substrate to generate volatile gases; otherwise, the chemical reaction cannot continue. Wet etching is widely used in the semiconductor industry, which requires etching of the substrate material.

In the process under development, irradiation of reactive plasma was employed to modify the surfaces of a chemical inert material to form a more active layer. Subsequently, acid etching was used to preferentially remove the active layer. Figure 1 shows a schematic of PaE process. After hydrogen with a flow rate of 30 standard-state cubic centimeters per minute (cm^3/min) was supplied to the Diener plasma generator, some hydrogen was excited, becoming reactive radicals at radio frequency (RF) (f = 13.56 MHz). The reactive radicals caused chemical reactions with the surface atoms. As a result, hydrogen ions were introduced into the sesquioxide, transforming it into hydroxide. Additionally, hydroxide is more likely to react with acids than sesquioxide. After plasma modification, inorganic acid was used to remove the modified layer to obtain an

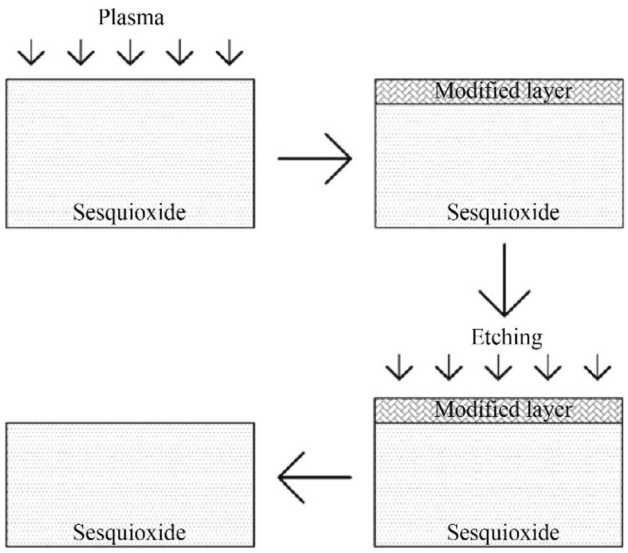

Fig. 1 Schematic of plasma-assisted etching

Table 1 Experimental parameters in plasma-assisted etching

Parameters	Conditions
Process gas	H_2
Flow rate/($cm^3 \cdot min^{-1}$)	30
RF power/W	90
Plasma processing time/h	2
Inorganic acid	HNO_3
Etching processing time/h	1

ultrasmooth surface without surface/subsurface damage. The experimental parameters are listed in Table 1.

3 Experimental investigations

3.1 Plasma modification process

XPS and TEM were employed in this experiment to investigate the modified surfaces and confirm the generation of a reacted layer on Lu_2O_3 with hydrogen plasma. Figures 2a, b show the X-ray photoelectron spectra of the processed surfaces, which correspond to Lu 4f and O 1s, respectively. Subfigures (i), (ii), and (iii) of Fig. 2a, b show the surface before hydrogen plasma irradiation, the surface after hydrogen plasma irradiation, and the surface after PaE, respectively. The peaks corresponding to the Lu–O bond (7.5, 8.7, 529.7 and 532.5 eV) can be observed in Figs. 2a (i) and 2b (i) [27, 28]. The peaks observed at 10.4 eV and 531.6 eV were identified as the Lu–OH bond in Figs. 2a (ii) and 2b (ii), corresponding to Lu(OH)*x*, a mixture of LuOOH and $Lu(OH)_3$ [28–30]. These results indicate that the irradiation of hydrogen plasma converted the sesquioxide into hydroxide on the surface of Lu_2O_3, and it is thought that the hydrogenation species in this reaction system was hydrogen radical because only hydrogen gas was used to excite the plasma. After PaE, the peak intensity of the Lu–OH bond disappeared, as shown in Figs. 2a (iii) and 2b (iii). Additionally, it is thought that the inorganic acid removed the modified layer easily. The main chemical reaction in this process is described as follows.

$$Lu_2O_3 + H^* \longrightarrow Lu(OH)_x \quad (1)$$

$$Lu(OH)_x + H^+ \longrightarrow Lu^{3+} + H_2O \quad (2)$$

TEM is a very direct and clear way to observe subsurface changes. Figure 3 shows the TEM analysis of the Lu_2O_3 surface before and after irradiation by hydrogen plasma for 2 h, and the illustration is the fast Fourier transform (FFT) pattern for the white selected area [31–33]. The modified layer was covered by a Pt layer to protect it during the focused ion beam fabrication process. As shown in the low-resolution TEM images in Figs. 3a and b, a modified layer with a thickness of approximately 65 nm was generated after the plasma treatment. In the high-resolution TEM images and FFT pattern in Fig. 3, the Lu_2O_3 crystals changed from a homogeneous lattice to a disordered lattice after the hydrogen plasma treatment.

By combining the characterization results of TEM and XPS, it can be proved that the modified layer was formed

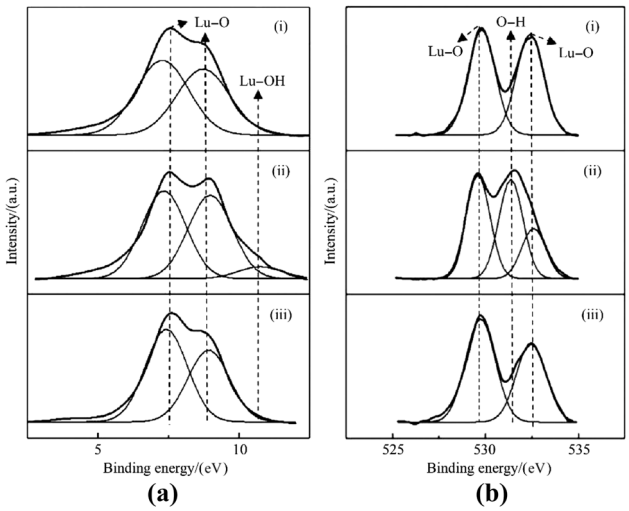

Fig. 2 XPS spectra of the processed Lu_2O_3 surfaces, which correspond to **a** Lu $4f_{7/2}$, **b** O 1s ((i) before plasma treatment, (ii) after plasma treatment, (iii) after acid etching)

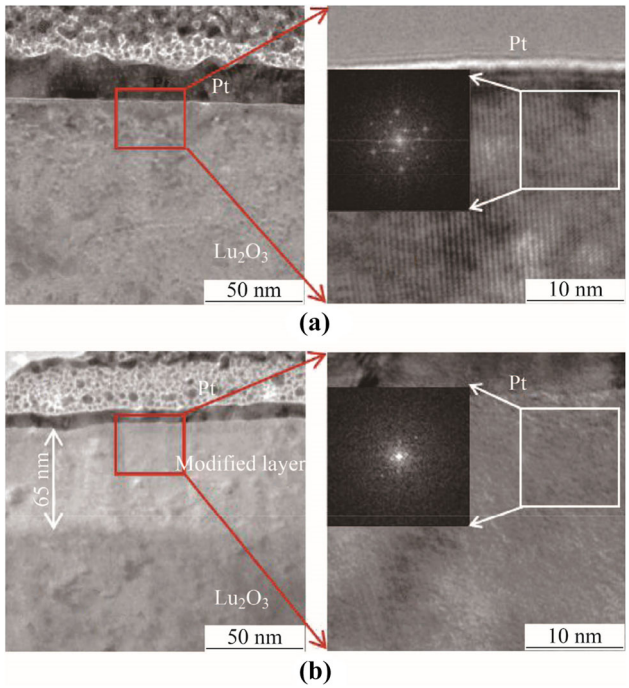

Fig. 3 TEM images of Lu_2O_3 surface **a** before plasma treatment, **b** irradiated by hydrogen plasma for 2 h

by converting oxides into hydroxides, and the thickness of the modified layer was 65 nm.

3.2 Acid etching process

Lutetium oxide crystals have strong chemical inertia and extremely low reaction rates with acid. Figure 4 shows the two-dimensional (2-D) white light interferometry (WLI) image of morphological changes after the reaction of lutetium oxide with nitric acids or aqua regia for 1 h. The three 2-D contour curves are almost identical, which indicates that Lu_2O_3 hardly reacts with these two acids.

Copper tape was used to cover half of the sample before plasma treatment to observe the removal effect after PaE. Then, the copper tape was removed and the modified Lu_2O_3 sample was etched with HNO_3 to remove the modified layer. The etching results were obtained by comparing the surfaces before and after HNO_3 etching, as shown in Figs. 5 and 6. A boundary between the modified area and the nonmodified area can be observed in Fig. 5. The gradual disappearance of scratches from the non-modified area to the modified area indicates the effectiveness of the etching removal. The high-magnification SEM image in Fig. 5 shows that numerous scratches are exposed at the boundary. This could be the subsurface damage from previous processing which was exposed after PaE processing, and the scratches in the PaE processing area may have disappeared. Figure 6 shows a WLI image of the Lu_2O_3 sample, where the height of the modified area is lower than that of the nonmodified area by 25.7 nm. Moreover, increasing the acid etching time and changing the type of acid did not result in the removal of samples, proving the feasibility of PaE.

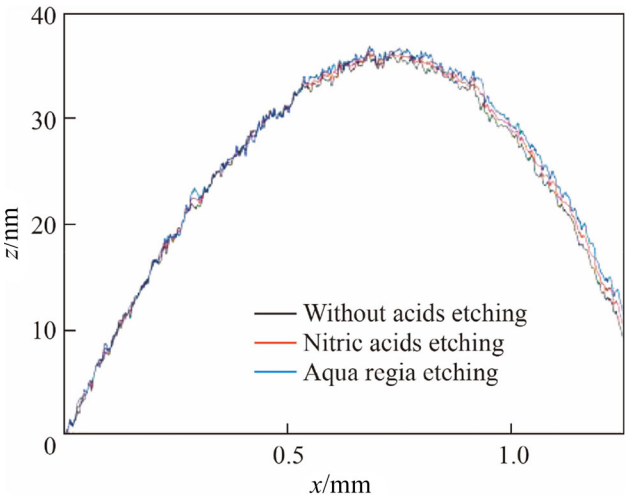

Fig. 4 2-D WLI image of Lu_2O_3 after etching

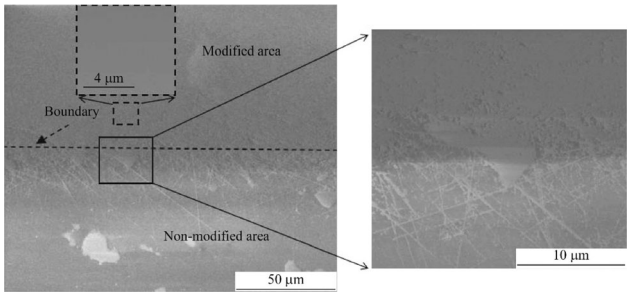

Fig. 5 SEM images of the Lu_2O_3 surface processed by PaE

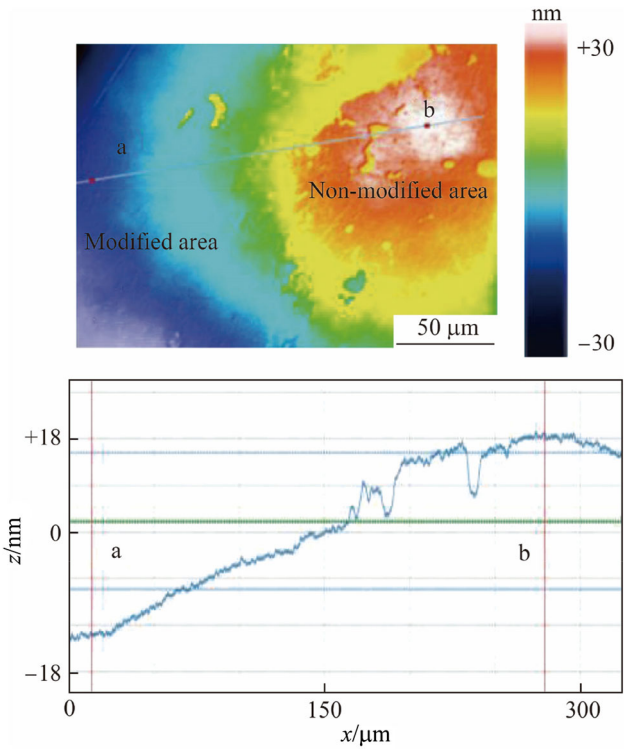

Fig. 6 Etching boundary of Lu_2O_3 wafer by HNO_3 for 1 h

3.3 Surface and subsurface damage

To maximize the crystal laser performance, the application of Lu_2O_3 substrates requires not only a flat surface with no scratches, but also no subsurface damage. The surface quality of Lu_2O_3 substrates is guaranteed after chemical-mechanical polishing. An ultraprecision lathe was used to carve crosslines on the surface of the Lu_2O_3 sample, thus ensure repeatability of the measurement position. As shown in Fig. 7, an area of 50 μm × 50 μm at 200 μm from the center of the crossline was selected as the marked area. Figure 8 shows the WLI and SEM images of the processed surface in the marked area; the surface roughness decreased slightly from 0.40 nm to 0.38 nm. Therefore, a flat surface can be guaranteed after PaE treatment. As for the subsurface damage, the scratches on the boundary

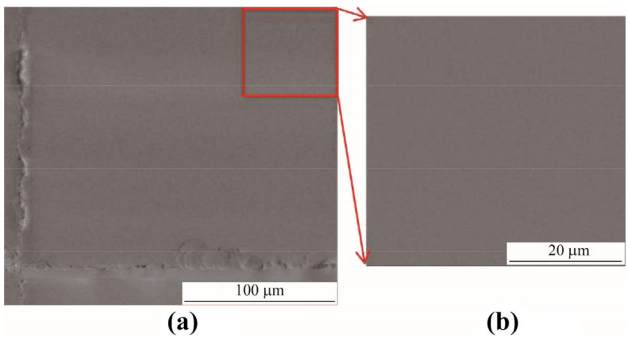

Fig. 7 SEM images of the marking point on Lu_2O_3 surface **a** cross line area, **b** marked measuring area

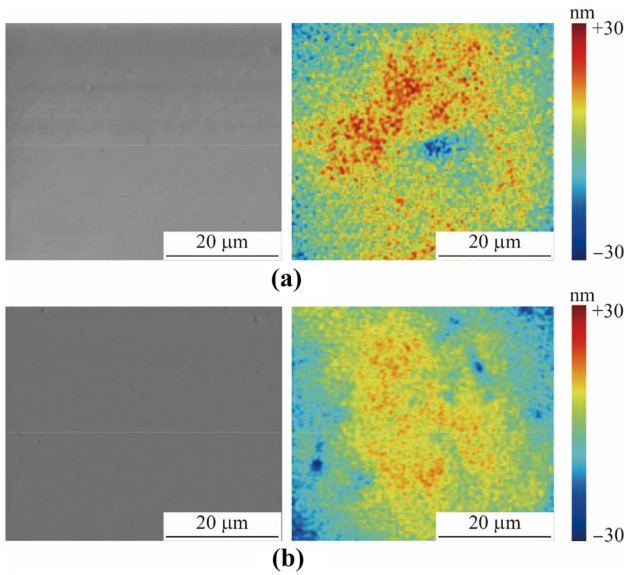

Fig. 8 SEM and WLI images of Lu_2O_3 surface at the marked point **a** before PaE processing the arithmetical mean height of the surface (Sa) 0.40 nm, **b** after PaE processing Sa 0.38 nm

between the modified and unmodified areas in Fig. 5 imply subsurface damage exposure after inorganic acid etching. The subsurface damage of Lu_2O_3 can be evaluated by TEM observation. However, the measurement range of TEM is quite small.

Raman spectroscopy is a nondestructive and efficient analysis method for characterizing subsurface damage [34]. This technique was used to characterize subsurface damage of marked areas before plasma treatment, after plasma treatment, and after acid etching; the results are shown in Fig. 9. The surface of Lu_2O_3 was modified with a layer of approximately 65 nm, as shown in Fig. 3c. In contrast, the Raman (532 nm laser) resolution depth was much higher than the layer thickness; the modified layer on the surface significantly affected the monocrystalline properties and the peaks decreased. The Raman peaks were higher after inorganic acid etching than before plasma treatment,

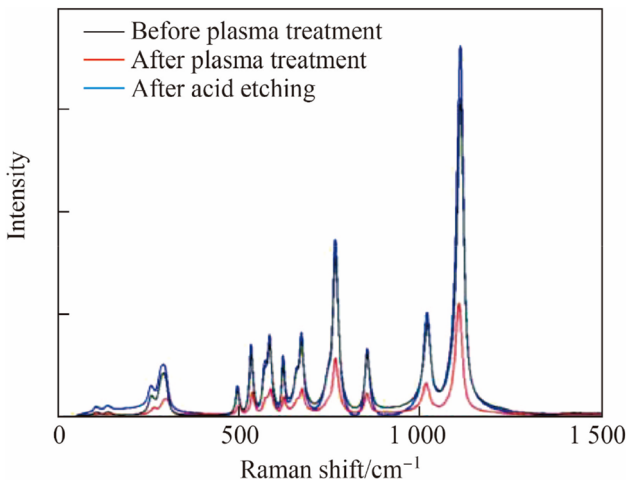

Fig. 9 Raman spectra of Lu_2O_3 under different treatment conditions collected with 532 nm laser

indicating that the modified layer and the subsurface damages were both removed. Meanwhile, the disappearance of the XPS peak intensities of the Lu–OH bond after acid etching indicates that the modified layer can be removed easily, which means that an atomically flat Lu_2O_3 surface is obtained.

4 Conclusions

A nanometric finishing approach combining irradiation of hydrogen plasma with inorganic acid etching was proposed to achieve high-integrity Lu_2O_3 surfaces without introducing subsurface damage. The results of the XPS and TEM measurements show that the irradiation of hydrogen plasma thoroughly converted the sesquioxide into hydroxide. The SEM, WLI, and Raman spectroscopy results indicate that the irradiation of hydrogen plasma increases the etching rate of Lu_2O_3 without introducing scratches or crystallographic subsurface damage. The experimental investigation reveal that PaE can achieve an atomically smooth surface in finishing a Lu_2O_3 substrate without introducing scratches or subsurface damage.

Acknowledgements This work was supported by the National Key Research & Development Program (Grant No. 2016YFB1102203), the National Natural Science Foundation of China (Grant No. 61635008), the "111" project by the State Administration of Foreign Experts Affairs and the Ministry of Education of China (Grant No. B07014), and the National Science Fund for Distinguished Young Scholars (Grant No. 51605327).

Open Access This article is licensed under a Creative Commons Attribution 4.0 International License, which permits use, sharing, adaptation, distribution and reproduction in any medium or format, as long as you give appropriate credit to the original author(s) and the source, provide a link to the Creative Commons licence, and indicate

if changes were made. The images or other third party material in this article are included in the article's Creative Commons licence, unless indicated otherwise in a credit line to the material. If material is not included in the article's Creative Commons licence and your intended use is not permitted by statutory regulation or exceeds the permitted use, you will need to obtain permission directly from the copyright holder. To view a copy of this licence, visit http://creativecommons.org/licenses/by/4.0/.

References

1. Chan VWS (2002) Optical space communications. IEEE J Sel Top Quantum Electron 6:959–975
2. Taczak TM, Killinger DK (1998) Development of a tunable, narrow-linewidth, cw 2.066-μm Ho:YLF laser for remote sensing of atmospheric CO_2 and H_2O. Appl Opt 37:8460–8476
3. Gattass RR, Mazur E (2008) Femtosecond laser micromachining in transparent materials. Nat Photonics 2:219–225
4. Flock ST, Stern T, Lehman P et al (1997) Er:YAG laser-induced changes in skin in vivo and transdermal drug delivery. Proc SPIE Int Soc Opt Eng 2970:374–379
5. Boulnois JL (1986) Photophysical processes in recent medical laser developments: a review. Lasers Med Sci 1:47–66
6. Weber MJ (1968) Radiative and multiphonon relaxation of rare-earth ions in Y_2O_3. Phys Rev 171:283–291
7. Petermann K, Huber G, Fornasiero L et al (2000) Rare-earth-doped sesquioxides. J Lumin 87:973–975
8. Koopmann P, Lamrini S, Scholle K et al (2011) Multi-watt laser operation and laser parameters of Ho-doped Lu_2O_3 at 2.12 μm. Opt Mater Express 1:1447–1456
9. Fornasiero L, Mix E, Peters V et al (1999) New oxide crystals for solid state lasers. Cryst Res Technol 34:255–260
10. Boulon G (2003) Yb^{3+} doped oxide crystals for diode-pumped solid state lasers: crystal growth, optical spectroscopy, new criteria of evaluation and combinatorial approach. Opt Mater 22:85–87
11. Peters V, Bolz A, Petermann K et al (2002) Growth of high-melting sesquioxides by the heat exchanger method. J Cryst Growth 237:879–883
12. Mun JH, Novoselov A, Yoshikawa A et al (2005) Growth of Yb^{3+}-doped Y_2O_3 single crystal rods by the micro-pulling-down method. Mater Res Bull 40:1235–1243
13. Fang FZ, Zhang N, Guo D et al (2019) Towards atomic and close-to-atomic scale manufacturing. Int J Extreme Manuf 1:012001
14. Fang FZ (2020) Atomic and close-to-atomic scale manufacturing: perspectives and measures. Int J Extreme Manuf 2:030201
15. Li C, Wu Y, Li X et al (2019) Deformation characteristics and surface generation modelling of crack-free grinding of GGG single crystals. J Mater Process Technol 279:116577
16. Fang FZ, Xu F (2018) Recent advances in micro/nano-cutting: effect of tool edge and material properties. Nanomanuf Metrol 1:4–31
17. Nagano M, Yamaga F, Zettsu N et al (2011) Development of fabrication process for aspherical neutron focusing mirror using numerically controlled local wet etching with low-pressure polishing. Nucl Instrum Methods Phys Res 634:112–116
18. Namba Y, Tsuwa H (1977) Ultrafine finishing of sapphire single crystal. CIRP Ann 26:325–329
19. Mori Y, Yamauchi K, Endo K (1987) Elastic emission machining. Precis Eng 9:123–128
20. Gormley J, Manfra M, Calawa A (1991) Hydroplane polishing of semiconductor crystals. Rev Sci Instrum 52:1256–1259
21. Li ZJ, Qin Z, Zhou ZH et al (2009) SnO_2 nanowire arrays and electrical properties synthesized by fast heating a mixture of SnO_2 and CNTs waste soot. Nanoscale Res Lett 4:1434–1438
22. Kordonski VW, Golini D, Dumas P et al (1998) Magnetorheological-suspension-based finishing technology. Proc SPIE-Int Soc Opt Eng 3326:527–535
23. Yang X, Yang XZ, Sun RY et al (2019) Obtaining atomically smooth 4H-SiC (0001) surface by controlling balance between anodizing and polishing in electrochemical mechanical polishing. Nanomanuf Metrol 2:140–147
24. Arnold T, Böhm G, Fechner R et al (2010) Ultraprecision surface finishing by ion beam and plasma jet techniques-status and outlook. Nucl Instrum Methods Phys Res B 616:147–156
25. Sun RY, Yang X, Watanabe K et al (2019) Etching characteristics of quartz crystal wafers using argon-based atmospheric pressure CF_4 plasma stabilized by ethanol addition. Nanomanuf Metrol 2:168–176
26. Yamamura K, Takiguchi T, Ueda M et al (2011) Plasma assisted polishing of single crystal SiC for obtaining atomically flat strain-free surface. CIRP Ann Manuf Technol 60:571–574
27. Mondal S, Her JL, Koyama K et al (2014) Resistive switching behavior in Lu_2O_3 thin film for advanced flexible memory applications. Nanoscale Res Lett 9:3
28. Espinós JP, González-Elipe AR, Odriozola JA (1987) XPS study of lutetium oxide samples with different hydration/carbonation degrees as a function of the preparation method. Appl Surf Sci 29:40–48
29. Päiväsaari J (2007) Atomic layer deposition of rare earth oxides. Top Appl Phys 106:15–32
30. Pan TM, Lin CW (2011) Structural and sensing properties of high-*k* Lu_2O_3 electrolyte-insulator-semiconductor pH sensors. J Electrochem Soc 158:J96
31. Fukushima Y, Ikoma Y, Edalati K et al (2017) High-resolution transmission electron microscopy analysis of bulk nanograined silicon processed by high-pressure torsion. Mater Charact 129:163–168
32. Knoop LD, Kuisma MJ, Löfgren J et al (2019) Electric field-induced surface melting of gold observed in situ at room temperature and at atomic resolution using TEM. Microsc Microanal 25:1830–1831
33. Gan Z, Hu G, Peng Z et al (2019) Surface modification of $LiNi_{0.8}Co_{0.1}Mn_{0.1}O_2$ by WO_3 as a cathode material for LIB. Appl Surf Sci 481:1228–1238
34. Ubaldini A, Carnasciali MM (2008) Raman characterisation of powder of cubic RE_2O_3 (RE = Nd, Gd, Dy, Tm, and Lu), Sc_2O_3 and Y_2O_3. J Alloys Compd 454:374–378

Peng Lyu is a Ph.D. candidate at the Centre of Micro/Nano Manufacturing Technology (MNMT), Tianjin University. He received the B.Eng. degree in Mechanical Manufacturing and Automation from Southeast University in 2016. His research interest is ultra-precision polishing.

Min Lai is a lecturer from Tianjin University and the member in the Centre of Micro/Nano Manufacturing Technology (MNMT). She received her Ph.D. from Tianjin University in 2016. Her main research interests focus on the ultra-precision machining mechanisms and micro/nano manufacturing technology.

Feng-Zhou Fang is a joint professor and the director of Centre of Micro/Nano Manufacturing Technology (MNMT) in both Tianjin University and University College Dublin. He received his Ph.D. in Manufacturing Engineering from the Harbin Institute of Technology and has been working in the field of manufacturing since 1982. He has conducted both fundamental studies and application development in the areas of micro/nano machining, optical freeform design and manufacturing, and ultra-precision machining and measurement benefiting a variety of industries in medical devices, bio-implants, optics and mold sectors.